



Selective adsorption and identification of penicillin G sodium in milk by molecularly imprinted polymer doped carbon dot

Yi Xu¹ · Haiping Wang¹ · Qingyan Bai¹ · Shujuan Ma³ · Chunmiao Bo¹ · Junjie Ou^{2,3}

Received: 9 December 2023 / Accepted: 18 February 2024 / Published online: 7 March 2024
© The Author(s), under exclusive licence to Springer-Verlag GmbH Austria, part of Springer Nature 2024

Abstract

A carbon dot (CD) was prepared by *o*-phenylenediamine and water, which showed bright yellow fluorescence under ultraviolet light irradiation ($\lambda = 580$ nm), and verified good fluorescence quenching effect on penicillin G sodium (Png-Na). Using methacrylic acid as a functional monomer, ethylene glycol dimethacrylate as a crosslinker, and Png-Na as a template, a kind of composite microsphere combining CD and molecularly imprinted polymer (MIP) was synthesized by surface-initiated atomic transfer radical polymerization (SI-ATRP). For reasons of comparison, we also prepared MIP without CD and non-imprinted polymers (NIPs). Through static and dynamic adsorption experiments, the maximum adsorption capacity was 47.05 mg g^{-1} and the equilibrium time was 30 min. High-performance liquid chromatography (HPLC) was utilized to determine the content of Png-Na in the spiked milk samples. A sensitive, rapid, and simple method for determination of Png-Na in food samples was developed. The utilized approach enabled the quantification of Png-Na within the concentration range $20\text{--}1000 \text{ }\mu\text{g L}^{-1}$ (with a limit of detection of $5 \text{ }\mu\text{g L}^{-1}$). The recoveries achieved were in the range 93.3–98.2%, with a relative standard deviation of 1.2–4.2%. The results demonstrated that CD@MIP possessed the capability of specific adsorption and fluorescence detection of Png-Na, enabling simultaneous detection and enrichment of Png-Na in real samples.

Keywords Penicillin G sodium · Carbon dot · Molecularly imprinted polymer · Surface-initiated atomic transfer radical polymerization · High-performance liquid chromatography

Introduction

Antibiotic has been widely utilized in animal husbandry for over 50 years, primarily with the aim of preventing or treating diseases affecting animals, meaning that undesirable residues can pose a real risk to humans [1]. The discovery of penicillin G, the first β -lactam antibiotic, was a

major breakthrough in modern chemotherapy [2]. Penicillin G sodium (Png-Na) belongs to a penicillin class of antibiotics, mainly treating mastitis in dairy cows [3]. However, excessive and illegal use of Png-Na may cause the presence of resistant bacteria and drug residues in dairy products, which can cause allergic reactions in hypersensitive individuals, posing a risk to human health, such as sensitization or toxicological reactions [4–6]. Therefore, antibiotic residue analysis is of great significance to ensure food safety. European Union regulation 508/1999 sets a residue limit of $4 \text{ }\mu\text{g kg}^{-1}$ or $1.2 \times 10^{-8} \text{ mol L}^{-1}$ for penicillin in milk. The U.S. Food and Drug Administration sets the residual limit for penicillin G in milk at $5 \times 10^{-9} \text{ IU mL}^{-1}$ [7]. Chinese Ministry of Agriculture has set the residual limit of penicillin G in milk at $4 \text{ }\mu\text{g L}^{-1}$. In order to suppress the irrational use of antibiotics and the emergence of drug-resistant strains, it is of great significance to develop a simple and sensitive detection method for detection of antibiotic residues in food [8]. Current methods for detecting Png-Na include high-performance liquid chromatography (HPLC) [9], gas chromatography-mass spectrometry [10],

✉ Chunmiao Bo
bocm-001@163.com

✉ Junjie Ou
junjieou@nwu.edu.cn; junjieou@dicp.ac.cn

¹ School of Chemistry and Chemical Engineering, Key Laboratory for Chemical Engineering and Technology, State Ethnic Affairs Commission, North Minzu University, Yinchuan 750021, China

² College of Chemistry and Materials Science, Northwest University, Xi'an 710127, China

³ CAS Key Laboratory of Separation Science for Analytical Chemistry, Dalian Institute of Chemical Physics, Chinese Academy of Sciences, Dalian 116023, China

liquid chromatography-tandem mass spectrometry [11], and surface-enhanced Raman spectroscopy [12]. These methods offer several advantages, including high sensitivity, good selectivity, and fast detection speed. However, they do have limitations, such as the need for complex sample preparation and the use of toxic organic solvents, resulting in long processing times and potential safety concerns [13]. It is still necessary to develop novel method to fast and sensitive detect Png-Na.

Molecularly imprinted polymers (MIPs) have broad prospects in the field of separation and enrichment due to their simplicity, reliability, and high adsorption to specific template molecules [14]. Compared to other methods, molecular imprinting technology can produce polymers with specific recognition capabilities, allowing for rapid and efficient separation of target substance [15]. In recent years, the composite material prepared by the combination of imprinting material and carbon dot (CD) has been developed because of its many advantages [16]. However, traditional synthetic methods usually result in the template molecules being wrapped in MIP, which hinders the binding dynamics [17]. Surface-initiated atomic transfer radical polymerization (SI-ATRP) has the advantages of controllable chain segment, wide selection of monomers, mild reaction conditions, and easy operation, which effectively solve some limitations of traditional polymerization methods [18]. The surface of the MIP prepared by SI-ATRP has many recognition sites, which not only improves the recognition efficiency, but also prevents the leakage of template molecules, so it has a great application prospect [19]. Li et al. prepared a magnetic surface imprinting material with good selectivity to cephalixin by SI-ATRP and successfully applied it in detection of trace residues from tap water and milk samples, showing excellent enrichment effect [20].

As a new nanomaterial derived from carbon material, CD exhibits good stability, superior water solubility, unique photoluminescence, and good biocompatibility [21, 22]. Depending on the carbon source, the fabrication methods of CD can be roughly divided into “top-down” and “bottom-up” synthesis [23]. Bottom-up methods include pyrolysis, hydrothermal method, and microwave-assisted method, and top-down methods include laser ablation method, arc discharge method, and electrochemical method [24]. It is widely used in high-sensitivity detection in biosensing because of its excellent properties, simple synthesis pathway, and adjustable surface function. In our case, a composite material of CD and MIP, named as CD@MIP, was prepared by SI-ATRP method using methacrylic acid (MAA) as functional monomer and ethylene glycol dimethacrylate (EDMA) as crosslinking agent. As a comparison, we also prepared MIP without CD as well as non-imprinted polymers (NIPs). Their adsorption capacity and properties of Png-Na were investigated by isothermal adsorption experiment and kinetic

adsorption experiment. Subsequently, the trace amount of Png-Na in milk samples and the enrichment ability of Png-Na in CD@MIP were determined by HPLC.

Experimental

Reagents and materials

Glycidyl methacrylate (GMA), *O*-phenylenediamine (*o*-PD), sulfuric acid, 2,2-azobisisobutyronitrile (AIBN), dichloromethane, triethylamine, 2-bromoisobutyryl bromide, ethanol, 4-dimethylaminopyridine, 2-2'-bipyridine (Bpy), ampicillin (AMP), amoxicillin (AMX), and Png-Na were purchased from Innochem (Beijing, China). MAA, EDMA, cuprous bromide (CuBr), ethylenediaminetetraacetic acid disodium salt (EDTA-2Na), glacial acetic acid, and oxalic acid dihydrate were provided by Aladdin Industries Co. (Shanghai, China). The above reagents were not further purified. Chromatographic grade acetonitrile was purchased from Damao (Tianjin, China). The milk was bought from the local supermarket (Yinchuan, China).

Characterization

Scanning electron microscopy (SEM) images were taken by JEM-7500F (JEOL-Japan). Fourier-transform infrared (FT-IR) were determined by Thermo Nicolet iS50 spectrometer (USA). X-ray photoelectron spectroscopy (XPS) was performed on an ESCALAB 250XI XPS spectrometer (Thermo Scientific, USA). The residual concentration was analyzed with an ultraviolet-visible (UV-VIS) spectrophotometer (TU-1950, China). The fluorescence spectrum of the material was analyzed by LS-55 fluorescence spectrometer (Shimadzu, Japan). Brunauer-Emmet-Teller analysis (BET, Tri star 3020, USA) was performed to analyze the specific surface area by nitrogen adsorption-desorption isotherm and pore size distribution.

Preparation of CD

According to previous report [25], yellowish CD was prepared by one-step hydrothermal polymerization. Typically, 500 mg of *o*-PD was dissolved in 50 mL of water, then the solution was sealed in a Teflon-lined autoclave and heated at 180 °C for 12 h. After natural cooling, the obtained suspension was passed through the 0.22- μ m membrane to remove the sediment, and CD suspension was obtained. Finally, the resulting CD suspension was dialyzed in a dialysis bag (1000 Da) and concentrated by rotary evaporation.

Preparation and modification of monodisperse poly(GMA-co-EDMA) microspheres

According to our previous report [26], monodisperse poly(GMA-co-EDMA) microspheres were prepared by one-step seeded swelling polymerization. Then 3 g of poly(GMA-co-EDMA) microspheres was dispersed in 0.1 mol L⁻¹ sulfuric acid solution, and the reaction was reflux at 60 °C for 6 h. The products were washed with distilled water to neutral. The hydrolyzed poly(GMA-co-EDMA) microspheres were then dispersed in dry dichloromethane solvent and stirred for 30 min in an ice bath. Then 1.6 mL of triethylamine was added, and 3.6 mL of 2-bromoisobutryl bromide and 20 mg of 4-dimethylaminopyridine were added drop by drop after stirring for 10 min. The reaction was carried out under ice bath conditions for 2 h and then transferred to room temperature for 24 h. After washing and vacuum drying, the brominated poly(GMA-co-EDMA) microspheres were obtained, which was assigned as poly(GMA-co-EDMA)-Br.

Preparation of MIP by SI-ATRP

First, ethanol (20 mL) and poly(GMA-co-EDMA)-Br (500 mg) were accurately weighed into a flask and sonicated to evenly disperse in the solvent. Then, Bpy (50 mg), Png-Na (178 mg), and MAA (0.063 mL) were added and dissolved by ultrasound. After EDMA (0.56 mL) and concentrated CD (1 mL) were added, the flask was sealed, frozen, evacuated, and thawed three times. Next, CuBr (25 mg) was quickly added under nitrogen, and further freezing, pumping, and thawing operations were performed three times, followed by reaction at 60 °C for 8 h under nitrogen protection. They were washed with ethanol, deionized water, and 0.1 mol L⁻¹ EDTA-2Na solution, successively, dried under vacuum for 12 h, and extracted with ethanol-glacial acetic acid (80/20, v/v) as eluent for 12 h by Soxhlet extraction. Finally, the composite material of CD and MIP (CD@MIP) was obtained by vacuum drying at 60 °C for 12 h.

Except that CD was not added, other steps were the same as above, and the resulting material was assigned as MIP.

Except that Png-Na and CD were not added, other steps were the same as above, and the acquired material was assigned as NIP.

Adsorption experiments

A certain amount of Png-Na was dissolved in ultrapure water to prepare the mother liquor (25 mg L⁻¹), which were diluted to obtain a series of standard solutions ranging from 1 to 25 mg L⁻¹. Absorbance curve was then measured with these standard solutions. Finally, 10 mg CD@MIP, MIP, or NIP was added to 200 mL of Png-Na standard solutions at

different concentrations (2, 4, 6, 8, 12, 16, 18, 21, 24 mg L⁻¹). The suspension solution containing the material were shaken at 25 °C and 200 r min⁻¹ for 3 h and filtered through a 0.22-μm filter membrane. The concentration of the remaining Png-Na was determined by UV-VIS spectrophotometer at 210 nm. The calculation formula of adsorption capacity Q_e is as follows:

$$Q_e = (C_o - C_e) \times V/m \quad (1)$$

where Q_e is the adsorption amount of Png-Na after adsorption balance, C_o and C_e are the initial and equilibrium concentration of Png-Na aqueous solution, V is the volume of Png-Na aqueous solution, and m is the mass of the material.

Isothermal adsorption curves are obtained by plotting the adsorption capacity Q_e for different concentrations of the Png-Na solution as a function of the initial concentration of the solution C_o , using the Langmuir model Eq. (2) and the Freundlich model Eq. (3):

$$C_e/Q_e = 1/Q_{\max}K_L + C_e/Q_{\max} \quad (2)$$

$$\lg Q_e = \lg K_F + \lg C_e/n \quad (3)$$

Here, Q_{\max} (mg g⁻¹) is the maximum adsorption capacity, and K_L and K_F are the adsorption constants of the Langmuir and Freundlich models, respectively.

The adsorption rate of Png-Na was studied by dynamic adsorption experiments. The 10 mg CD@MIP, MIP, or NIP was weighed and added into 200 mL solution (18 mg L⁻¹), respectively. After shaking at 25 °C for 5, 10, 15, 20, 30, 60, 90, and 120 min, the post-oscillation solution was filtered through a 0.22-μm aqueous membrane. Then the absorbance of the solution was measured on the UV-VIS spectrophotometer, and the adsorption capacity Q was calculated according to the standard curve. Curve was drawn with time as the abscissa and adsorption capacity as the ordinate. Equilibrium adsorption of Png-Na was calculated using Eq. (1), and the kinetic curves were fitted using the pseudo-first-order and pseudo-second-order models in Eqs. (4) and (5), respectively.

$$\ln(Q_e - Q_t) = \ln Q_e - k_1 t \quad (4)$$

$$t/Q_t = t/Q_e + 1/k_2 Q_e^2 \quad (5)$$

Here, Q_t (mg g⁻¹) is the adsorption amount of Png-Na at a given time point, and k_1 and k_2 are the rate constants of the pseudo-first-order and pseudo-second-order kinetic model equations, respectively.

Since AMP, AMX, and Png-Na are all veterinary drugs with similar structures, the adsorption capacities of AMP and AMX were measured to evaluate the adsorption capacity of CD@MIP. Firstly, 100 mL solution of AMP, AMX,

and Png-Na (18 mg L^{-1}) was prepared, respectively. Then, 10 mg of CD@MIP 10 mg was added to the solution containing AMP, AMX, and Png-Na in a water bath oscillator at room temperature and oscillated at 200 r min^{-1} for 120 min. After oscillation, the solution was filtered by $0.22\text{-}\mu\text{m}$ membrane, and the residual amount was determined by UV–VIS spectrophotometer at $\lambda = 235, 254, \text{ and } 210 \text{ nm}$. The equilibrium adsorption capacity is calculated by Eq. (1).

Fluorescence experiment

CD@MIP (50 mg) and Png-Na (10 mg) were weighed to prepare a material suspension of 50 mg L^{-1} and Png-Na solutions with different concentrations for fluorescence detection. CD@MIP suspension (1 mL) and CD solution (1 mL) were added to different concentrations of Png-Na solution (9 mL) and shook to mix well. The mixture was kept at room temperature for 5 min. The excitation wavelength was set at 410 nm, and the fluorescence intensity was determined by fluorescence spectrophotometry.

Determination of Png-Na in actual milk samples by HPLC

Milk was purchased from a nearby supermarket (Yinchuan, China). One gram of milk was weighed into a centrifuge tube. Png-Na solution was added, and then appropriate tetrabutylammonium bromide/acetonitrile solution (3.2 g L^{-1}) was also added. The spiked samples with concentrations of 4, 6, or $10 \text{ }\mu\text{g L}^{-1}$ were obtained. It was gently shook well, centrifuged at 8000 r min^{-1} for 5 min, and

the supernatant was acquired and assigned as spiked milk samples. CD@MIP (60 mg) was weighed into a solid-phase extraction (SPE) column and activated with 3 mL methanol and 3 mL water, successively. Then 10 mL of spiked milk samples was passed through the SPE column and rinsed with 5 mL of water. The flow rate was controlled at about 1 mL min^{-1} . Eluent was finally eluted with 1 mL methanol and glacial acetic acid (60/40, v/v), and the filtrate was analyzed by HPLC.

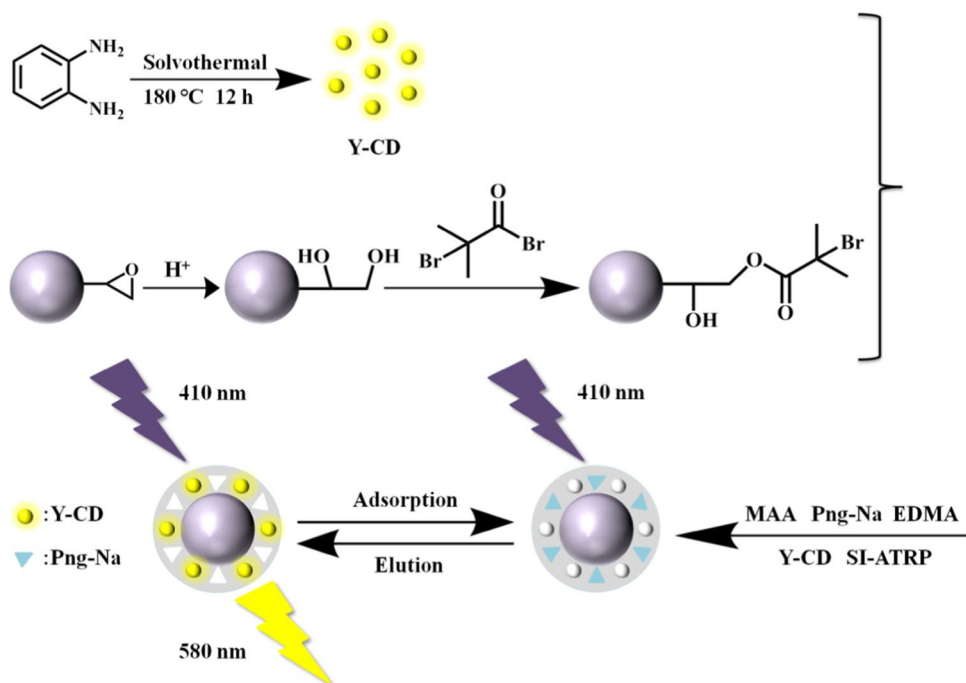
HPLC system consists of an SPD-20A UV–VIS spectrophotometer detector and two LC-20-AT pumps (Shimadzu Corporation, Japan). Chromatographic analysis was performed on a C18 column ($250 \times 4.6 \text{ mm}$, ODS, $5 \text{ }\mu\text{m}$) with mobile phase consisting of acetonitrile and disodium hydrogen phosphate aqueous solution (45/55, v/v). Flow rate was 1.0 mL min^{-1} , sample volume was $20.0 \text{ }\mu\text{L}$, column temperature was $25 \text{ }^\circ\text{C}$, and detection wavelength was 210 nm.

Results and discussion

Preparation of CD@MIP

In recent years, our research group has prepared several imprinted materials and bifunctional materials based on CD [27–29]. Therefore, the preparation of bifunctional composites with specific adsorption and fluorescence detection was still the focus of our research. As shown in Fig. 1, monodisperse poly(GMA-co-EDMA) microspheres were prepared by seed swelling polymerization according to our previous report [26]. Modified microspheres (acidizing, brominating)

Fig. 1 Synthetic schematic of CD@MIP



further served as matrix because of their good hydrophilicity and easy surface modification. Jalili et al. prepared a sensor using Y-CD and B-CD as a double fluorophore and MIP with mesoporous structure as a receptor for detection of Png [30]. In our work, Y-CD was also selected to prepare the bifunctional material for selective adsorption and identification of Png-Na via SI-ATRP, which exhibited excellent fluorescence quenching effect on Png-Na. This not only eliminates the modification of the surface primer group, but also simplifies the preparation process. The amino-containing CD was doped into MIP, while MAA could not only interact with CD through hydrogen bonding, but also copolymerize with EDMA on the surface of the microsphere to generate an imprinting layer.

Characterization of materials

First, poly(GMA-*co*-EDMA) microsphere, MIP and CD@MIP were examined by SEM. As shown in Fig. 2a and b, the spherical morphology of poly(GMA-*co*-EDMA) was observed, exhibiting excellent mono-dispersity, with a particle size of about 5.8 μm . Figure 2c and d present the morphology of the MIP material. In comparison to the poly(GMA-*co*-EDMA) microspheres, the surface of the MIP appeared to be rougher. This was due to the large number of imprinting sites covering the surface of microsphere. The morphology and size of CD@MIP particles, as depicted in Fig. 2e and f, also exhibited similarities to the pristine poly(GMA-*co*-EDMA) microspheres. CD@MIP was designed and fabricated as an imprinted polymer by adding both template molecules and CD. Therefore, it was also similar to MIP in morphology and size of about 5.8 μm .

BET analysis of poly(GMA-*co*-EDMA)-Br, MIP, and CD@MIP showed the nitrogen adsorption isotherm to

assess the specific surface area of the material. As observed from Fig. 3a, nitrogen adsorption further increases when the relative pressure exceeds 0.85, which indicates the presence of a large number of macropores in the material. These macropores would increase the mass transfer rate for fast adsorption. Figure 3b shows the pore diameter distributions. The specific surface area, pore volume, and average pore diameter of poly(GMA-*co*-EDMA)-Br, MIP, and CD@MIP are listed in Table 1. The specific surface areas of poly(GMA-*co*-EDMA)-Br, MIP, and CD@MIP were less than $10 \text{ m}^2 \text{ g}^{-1}$. Thus, the resulting CD@MIP exhibited less of micropores and mesopores.

FT-IR is adopted to characterize the functional groups on the surface of a material. FT-IR spectra of poly(GMA-*co*-EDMA), MIP, and CD@MIP are shown in Fig. 3c. The peak of epoxy group was observed at 910 cm^{-1} . However, this peak was absent in the spectra of both MIP and CD@MIP, indicating that the epoxy group was protonated via acidification reaction. It was observed that a peak at 660 cm^{-1} emerged in the spectra of MIP and CD@MIP, which was the absorption peak of bromine. This indicated that the bromine reaction was successful and bromine atoms were successfully introduced into the material. The tensile vibration of -OH group was located at 3544 cm^{-1} , and the adsorption peak of the -C=O group was located at 1730 cm^{-1} . Additionally, the characteristic peak at 1635 cm^{-1} was attributed to the tensile vibration of the -NH group, further demonstrating the introduction of CD into CD@MIP materials.

Through elemental analysis, it is possible to determine the changes in elemental content in different materials, further demonstrating the chemical changes during the preparation of materials and the introduction of functional groups. Poly(GMA-*co*-EDMA)-Br, MIP, and CD@MIP were characterized by elemental analysis, and the results are listed

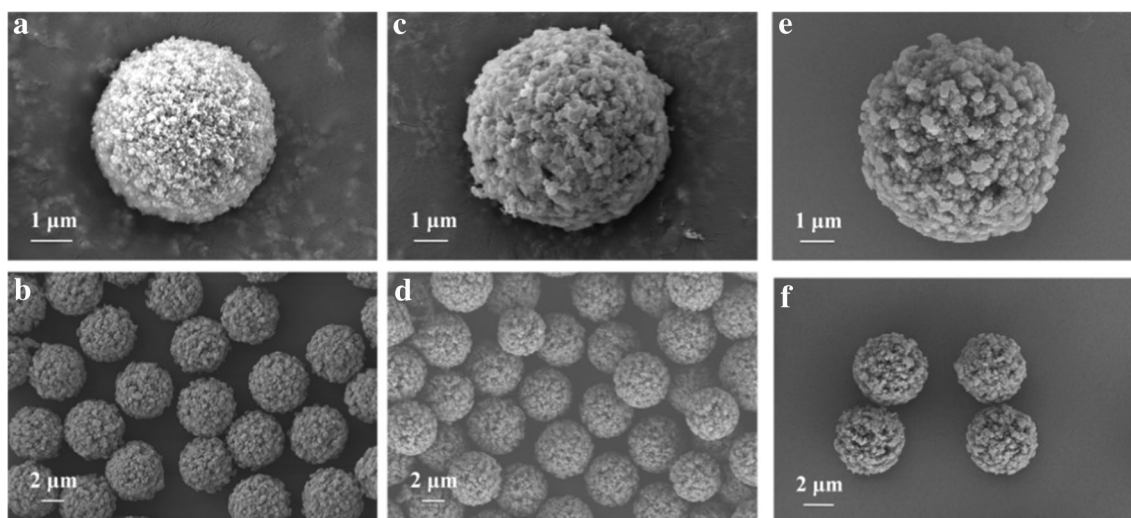


Fig. 2 SEM images of **a, b** poly(GMA-*co*-EDMA) sphere, **c, d** MIP, and **e, f** CD@MIP

Fig. 3 **a** Nitrogen sorption isotherms and **b** pore diameter distributions of poly(GMA-co-EDMA)-Br, CD@MIP and MIP, **c** FT-IR spectra of CD@MIP, MIP, and poly(GMA-co-EDMA)

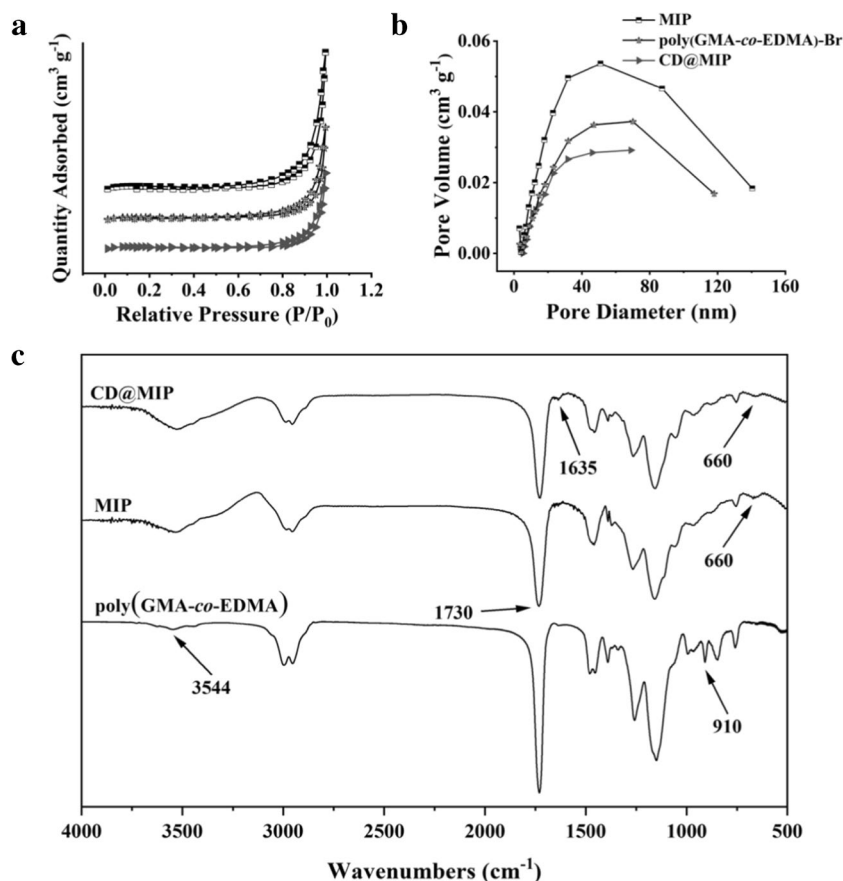


Table 1 Comparison of specific surface area, pore volume, and average pore diameter of poly(GMA-co-EDMA)-Br, MIP, and CD@MIP

Materials	Specific surface area (m ² g ⁻¹)	Pore volume (cm ³ g ⁻¹)	Average pore diameter (nm)
Poly(GMA-co-EDMA)-Br	6.6	0.054	33.0
MIP	4.5	0.037	32.4
CD@MIP	4.2	0.030	29.1

in Table S1. Compared with poly(GMA-co-EDMA)-Br (C, 48.61%; H, 4.83%), carbon (50.17%) and hydrogen (5.18%) elements of MIP were significant increased. This indicated that the crosslinker EDMA was successfully grafted onto the surface. The increase of nitrogen content (0.64%) in CD@MIP, compared with N (0.38%) of MIP, also indicated a successful integration of CD containing amino group into CD@MIP.

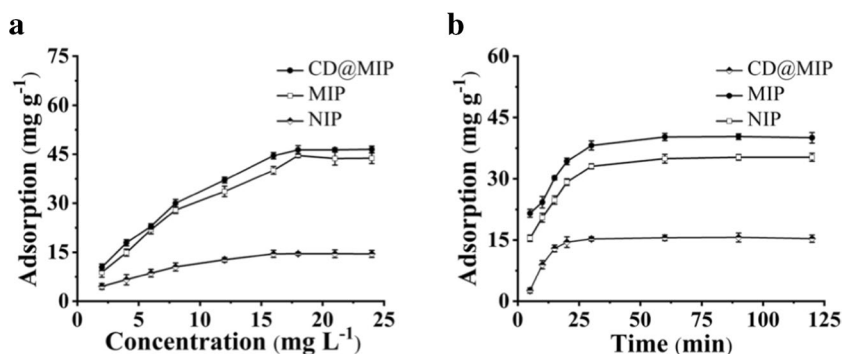
The existence of specific chemical bonds in the material can be obtained by XPS spectral analysis. As shown in Fig. S1a, these C, O, and N elements emerged in the full spectrum of CD@MIP. In Fig. S1b, c, and d, peaks of different energy levels were observed in high-resolution XPS

spectra. The peaks in the C 1 s spectrum in Fig. S1b are located at 284.8, 286.4, and 288.7 eV, representing the characteristic absorption peaks of C–C, C–O, and C=O, respectively. The presence of these peaks indicated the presence of the C–C, C–O, and C=O bonds in CD@MIP. The peak at 399.4 eV in Fig. S1c represented the characteristic absorption peak of amino N, which was consistent with the previously mentioned integration of the CD containing CD@MIP. O 1 s spectrum in Fig. S1d was located at 531.8 and 533.1 eV, representing the characteristic peaks of C=O and C–O, respectively. Based on the appearance of these peaks, it was determined that there are C=O and C–O bonds in CD@MIP.

Analysis of isothermal adsorption

The ability of the material to adsorb target is critical. Adsorption capacity of CD@MIP, MIP, and NIP for Png-Na solution with different concentrations were determined by adsorption experiment. The isothermal adsorption curves of CD@MIP, MIP, and NIP for Png-Na solutions are shown in Fig. 4a. When the concentration of Png-Na was ranged in 2–18 mg L⁻¹, the adsorption capacity of CD@MIP and MIP increased rapidly with an increase of the concentration of Png-Na, and then slowed down gradually, and the adsorption equilibrium

Fig. 4 Adsorption **a** isothermal and **b** kinetic curves of CD@MIP, MIP, and NIP



finally reached at the concentration of 18 mg L^{-1} . The saturated adsorption capacity of CD@MIP was 47.05 mg g^{-1} , and that of MIP was 43.76 mg g^{-1} . As the concentration of Png-Na increased from 2 to 16 mg L^{-1} , the adsorption capacity of NIP initially showed a rapid increase, followed by a gradual decrease. The adsorption equilibrium finally reached at a concentration of 16 mg L^{-1} for Png-Na. The saturated adsorption capacity of NIP was only 14.55 mg g^{-1} . These results indicated that CD@MIP, MIP, and NIP possessed somewhat ability to adsorb Png-Na. In a certain concentration range, the adsorption capacities of CD@MIP and MIP for Png-Na were significantly higher than that of NIP. This was due to the presence of an imprinting chamber in CD@MIP and MIP materials, which enabled specific recognition and adsorption of Png-Na. In contrast, NIP materials were not pre-treated with template molecules, so they cannot provide specific adsorption sites, resulting in low adsorption capacity. Adsorption capacity of CD@MIP was almost same to that of MIP. The addition of CD did not affect the adsorption capacity of MIP, but CD@MIP possessed the ability of fluorescence detection. As a result, CD@MIP and MIP could serve as selective materials for target adsorbents.

In order to study the adsorption mechanism of Png-Na, the isothermal adsorption curves of the materials were analyzed with Langmuir (Eq. 2) and Freundlich (Eq. 3) models. For MIP materials (Table S2), the linear correlation coefficient of Langmuir model was 0.9986, which was greater than the linear correlation coefficient of the Freundlich model (0.9843). This indicated that the adsorption mechanism of MIP materials for Png-Na was more fitted to the Langmuir model, which described the monolayer adsorption of molecules on the adsorption surface. According to Langmuir equation, there was a proportional relationship between adsorption capacity and adsorption concentration in solution. The applicability of Langmuir model indicated that the adsorption sites of MIP materials were limited and the adsorption layers were uniformly distributed during the adsorption process. On the other hand, the Freundlich model was widely adopted to describe heterogeneous adsorption systems where the relationship between adsorption capacity and adsorption concentration is nonlinear.

Study of adsorption kinetics

Adsorption kinetics was the key to evaluate the adsorption capacity of materials. Therefore, the adsorption kinetics of CD@MIP, MIP, and NIP for Png-Na at different concentrations were adopted. As the concentration of Png-Na increased, the adsorption capacities of three materials were rapidly increased within 30 min (Fig. 4b). After about 30 min, the adsorption process reached equilibrium. This finding further confirmed faster and more efficient performance of CD@MIP and MIP materials for Png-Na compared to NIP materials, which was attributed to the imprinting cavity in the surface of CD@MIP and MIP materials, thus achieving fast adsorption equilibrium.

In order to further investigate the adsorption kinetic mechanism, the pseudo-first-order kinetic model (Eq. 4) and pseudo-second-order kinetic model (Eq. 5) were adopted to fit the adsorption kinetic curve. In general, the pseudo-first-order kinetic model is assumed that the adsorption rate depends on the diffusion rate, while the pseudo-second-order kinetic model is assumed that chemical forces play a decisive role in the adsorption rate. It was observed from Table S3 that the adsorption curves of MIP conform to the pseudo-second-order kinetic adsorption model, indicating the existence of chemisorption process.

Comparison results with other related adsorption materials are shown in Table 2. Magnetic MIP (Mag-MIP) was synthesized via photopolymerization, which exhibited Png

Table 2 Comparison of several reported Png-Na adsorption materials

Materials	Maximum adsorption capacity (mg g^{-1})	Equilibrium time (min)	Ref
CD@MIP	47.04	30	This work
Mag-MIP	4.85	240	[31]
Nano-MIP	4.36	60	[32]
MgO nanoparticles	25.66	60	[33]
Hydrophilic gel	35	/	[34]
Modified activated carbon	140.8	540	[35]

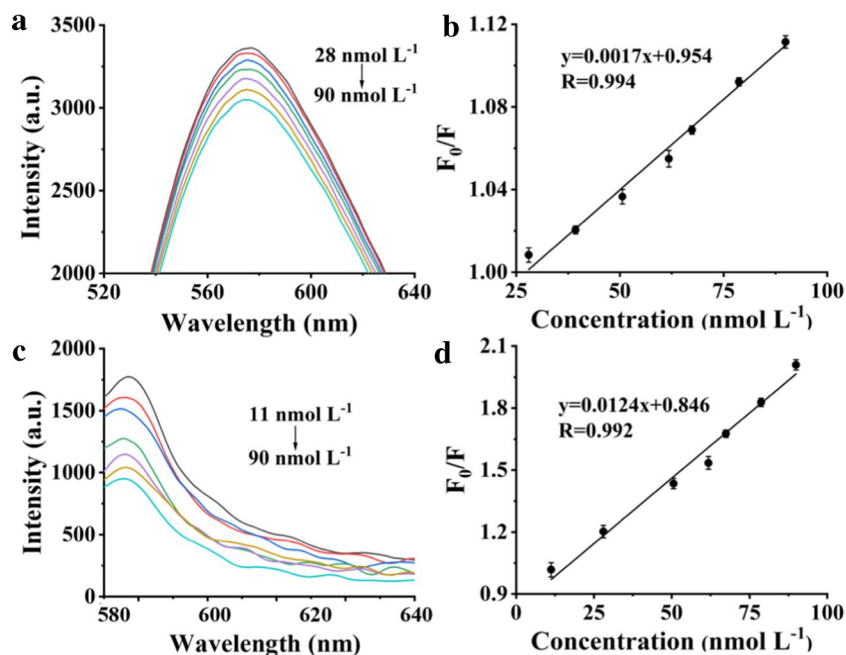
adsorption capacity of 4.85 mg g^{-1} and an equilibrium time of 240 min [31]. Rahim synthesized nanomolecular imprinted polymer (Nano-MIP) particles via microemulsion polymerization for selective identification of Png, with adsorption capacity of 4.36 mg g^{-1} and an equilibrium time of 60 min [32]. Rahdar investigated the adsorption performance of magnesium nanoparticles (MgO nanoparticles) to Png, with adsorption capacity of 25.66 mg g^{-1} and an equilibrium time of 60 min [33]. The adsorption of Png-Na on hydrophilic gel Toyopearl HW-40F with adsorption of 35 mg g^{-1} was also acquired [34], while the adsorption performance of thermally modified activated carbon for ampicillin revealed that the maximum adsorption capacity achieved was 140.85 mg g^{-1} with an equilibrium time of 540 min [35]. In our case, the CD@MIP exhibited a saturated adsorption capacity of 47.05 mg g^{-1} , and the adsorption equilibrium was achieved in 30 min. Adsorption capacity and adsorption rate were superior to those of Nano-MIP, MgO nanoparticles, and hydrophilic gel. Although the adsorption capacity of the modified activated carbon was better than that of CD@MIP, it took 540 min to reach the adsorption equilibrium.

To evaluate the specific recognition of Png-Na by CD@MIP, adsorption of a single sample was performed. As shown in Fig. S2, under the same conditions, the adsorption capacity of CD@MIP (47.05 mg g^{-1}) for Png-Na is significantly higher than those of AMP (16.07 mg g^{-1}) and AMX (10.49 mg g^{-1}), indicating that CD@MIP exhibited strong recognition specificity for Png-Na. This was attributed to the abundance of blotting sites on the surface of CD@MIP, which offered complementary blotting chambers specifically designed for Png-Na.

Fluorescence selectivity and sensitivity detection of Png-Na using CD@MIP

Fluorescence selectivity refers to the ability to accurately detect and differentiate the target analyte without interference from other substances. Figure 5a and b show a linear relationship between fluorescence intensity (F) and concentration (c) of Png-Na in the range of $28\text{--}90 \text{ nmol L}^{-1}$. For CD material, the fitting equation is $F_0/F = 0.0017[c] + 0.954$, and the correlation coefficient is 0.994. As shown in Fig. 5c and d, CD@MIP material also exhibited a linear relationship between fluorescence intensity and concentration of Png-Na in the range of $11\text{--}90 \text{ nmol L}^{-1}$. The fitting equation was $F_0/F = 0.0124[c] + 0.846$, and the correlation coefficient was 0.992. These results indicated that CD@MIP possessed high fluorescence quenching efficiency for Png-Na and good linear response. The quantum yield of CD was measured to be 10.2% by using quinine sulfate as fluorescence standard. Due to the strong interaction between Png-Na and CD@MIP, the excited state of CD is non-radiatively deactivated by electron transfer [30]. However, the ultraviolet absorption band of Png-Na was close to the band gap of CD, so the electrons in the CD conductive band could be directly transferred to the lowest unoccupied molecular orbital of the Png-Na ultraviolet band, resulting in fluorescence suppression of CD. These results demonstrated that both CD and CD@MIP exhibited high fluorescence quenching efficiency and selectivity to Png-Na. As a result, these materials would be applied in quantitative detection of Png-Na.

Fig. 5 Fluorescence emission spectra of **a** CD and **c** CD@MIP at different Png-Na concentrations, linear response curve for the detection of Png-Na by **b** CD and **d** CD@MIP



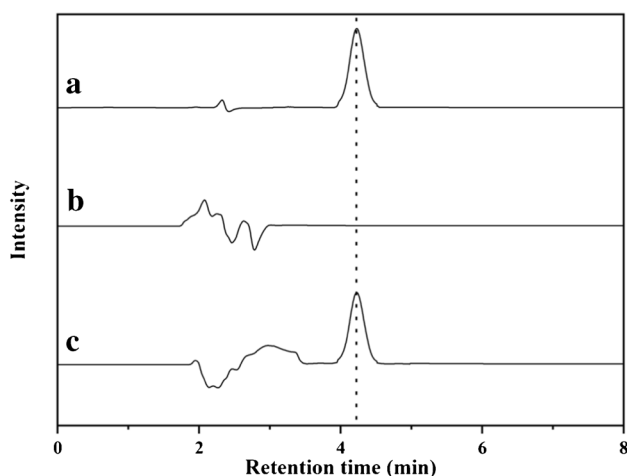


Fig. 6 Chromatograms of **a** standard sample of Png-Na, **b** milk actual sample, **c** sample after enrichment by CD@MIP

Analysis of actual samples in HPLC

In order to verify the enrichment ability of CD@MIP for Png-Na in milk samples, the eluent after SPE was analyzed by HPLC. Figure 6a presents chromatogram of standard Png-Na sample of $40 \mu\text{g L}^{-1}$, Fig. 6b presents the chromatogram of actual milk sample, while Fig. 6c shows the chromatogram of the milk sample spiked $4 \mu\text{g L}^{-1}$ of Png-Na and enriched with CD@MIP. The concentration reached $39.3 \mu\text{g L}^{-1}$ after enrichment. It was observed that CD@MIP exhibited a strong enrichment ability of Png-Na. By drawing the standard curve between the concentration of Png-Na standard solution and peak area, the linear equation was obtained as $y = 311.72x + 49.29$ ($R = 0.999$), which exhibited a good linear relationship in the concentration range of $20\text{--}1000 \mu\text{g L}^{-1}$. The limit of detection (LOD) was $5 \mu\text{g L}^{-1}$ based on triple signal-to-noise ratio, and the limit of quantitation (LOQ) was $17 \mu\text{g L}^{-1}$ based on ten times signal-to-noise ratio. Recovery rates of Png-Na and the intra-day and inter-day relative standard deviation (RSD, %, $n = 3$) of CD@MIP were tested to verify the repeatability of the experiment and evaluate its precision and accuracy. The results are shown in Table S4. Recoveries were ranged from 93.3 to 98.2%, while intra-day RSD ranged from 1.2 to 3.9%, and inter-day RSD ranged from 1.7 to 4.2%. These results demonstrated high accuracy and precision of CD@MIP in the detection and effective enrichment of Png-Na in milk samples. To verify that the template Png-Na was completely eluted, HPLC analysis of the eluent from CD@MIP was performed. As shown in Fig. S3, no absorption peak corresponding to Png-Na was observed, confirming that Png-Na was completely removed from CD@MIP.

Conclusion

In this study, a CD was synthesized, which exhibited a stable fluorescence quenching effect on Png-Na, and the poly(GMA-*co*-EDMA) as matrix and Png-Na as the template were utilized to synthesize CD-doped MIP (CD@MIP) by SI-ATRP. Combining the advantages of MIP and CD, the acquired CD@MIP possessed bifunctionality. First, the doping of CD did not affect the adsorption performance of CD@MIP, and it exhibited much higher adsorption and enrichment capacity for Png-Na compared to NIP. CD@MIP was applied in enrichment of Png-Na, and trace amount Png-Na in milk was successfully detected by HPLC. The method exhibited satisfactory stability, repeatability, and a high recovery rate. Second, the stable fluorescence quenching effect of CD@MIP could quantitatively analyze Png-Na. Third, the entire synthesis process of CD and CD@MIP was green and simple with excellent dispersion in the aqueous environment, making CD@MIP ideal for the adsorption and detection of Png-Na in real environments. In a word, CD@MIP possessed both specific adsorption and fluorescent detection of Png-Na, which can be widely applicable for the detection and enrichment of trace amounts of Png-Na in real samples.

Supplementary Information The online version contains supplementary material available at <https://doi.org/10.1007/s00604-024-06269-5>.

Acknowledgements Financial support is gratefully acknowledged from the CAS-Weigao Research & Development Program ([2017]-009) and the National Natural Sciences Foundation of Ningxia (No. 2021AAC02017) to J. Ou.

Funding This work was supported by National Natural Sciences Foundation of Ningxia, No. 2021AAC02017, Junjie Ou, The CAS-Weigao Research & Development Program, [2017]-009, Junjie Ou.

Data availability All data generated or analyzed during this study are included in this published article and its supplementary information files.

Declarations

Ethical approval This research did not involve human or animal samples.

Conflict of interest The authors declare no competing interests.

References

- Pennacchio A, Varriale A, Scala A, Marzullo VM, Staiano M, D'Auria S (2016) A novel fluorescence polarization assay for determination of penicillin G in milk. *Food Chem* 190:381–385
- Jiang X, Qin X, Yin D, Gong M, Yang L, Zhao B, Ruan W (2015) Rapid monitoring of benzylpenicillin sodium using Raman and

- surface enhanced Raman spectroscopy. *Spectrochim Acta A* 140:474–478
3. Thavarungkul P, Dawan S, Kanatharana P, Asawatreratanakul P (2007) Detecting penicillin G in milk with impedimetric label-free immunosensor. *Biosens Bioelectron* 23:688–694
 4. El-Moghazy AY, Zhao C, Istamboulie G, Amaly N, Si Y, Noguier T, Sun G (2018) Ultrasensitive label-free electrochemical immunosensor based on PVA-co-PE nanofibrous membrane for the detection of chloramphenicol residues in milk. *Biosens Bioelectron* 117:838–844
 5. Cao Y, Su X, Wang Q, Xue H, Zhu X, Zhang C, Jiang J, Qi S, Gong X, Zhu X, Pan M, Ren H, Hu W, Wei Z, Tian M, Liu W (2017) A multicenter study evaluating ceftriaxone and benzathine penicillin G as treatment agents for early syphilis in Jiangsu, China. *Clin Infect Dis* 65:1683–1688
 6. Luton E, Memphis M (1964) Methicillin tolerance after penicillin G anaphylaxis. *JAMA* 190:151–152
 7. Karageorgou E, Christoforidou S, Ioannidou M, Psomas E, Samouris G (2018) Detection of beta-Lactams and chloramphenicol residues in raw milk-development and application of an HPLC-DAD method in comparison with microbial inhibition assays. *Foods* 7:82
 8. Norzaee S, Taghavi M, Djahed B, KordMostafapour F (2018) Degradation of penicillin G by heat activated persulfate in aqueous solution. *J Environ Manage* 215:316–323
 9. Zhou S, Wang D, Zhao Y, Wu Y (2015) A rapid HPLC method for indirect quantification of beta-lactamase activity in milk. *J Dairy Sci* 98:2197–2204
 10. Santos R, Limas E, Sousa M, da Conceição CM, Ramos F, da Silveira MIN (2007) Optimization of analytical procedures for GC-MS determination of phytosterols and phytostanols in enriched milk and yoghurt. *Food Chem* 102:113–117
 11. Delatour T, Savoy M-C, Tarres A, Bessaire T, Mottier P, Desmarchelier A (2018) Low false response rates in screening a hundred veterinary drug residues in foodstuffs by LC-MS/MS with analyte-specific correction of the matrix effect. *Food Control* 94:353–360
 12. Andreou C, Mirsafavi R, Moskovits M, Meinhart CD (2015) Detection of low concentrations of ampicillin in milk. *Analyst* 140:5003–5005
 13. Wang Y, Zhang X, Pan Y, Chen Y (2017) Analysis of oil content in drying petroleum sludge of tank bottom. *Int J Hydrogen Energ* 42:18681–18684
 14. Hao HX, Zhou H, Chang J, Zhu J, Wei TX (2011) Molecularly imprinted polymers for highly sensitive detection of morphine using surface plasmon resonance spectroscopy. *Chinese Chem Lett* 22:477–480
 15. Madikizela LM, Tavengwa NT, Tutu H, Chimuka L (2018) Green aspects in molecular imprinting technology: from design to environmental applications. *Trends Environ Anal* 17:14–22
 16. Keçili R, Hussain CG, Hussain CM (2023) Emerging trends in green carbon dots coated with molecularly imprinted polymers for sensor platforms. *Trac-Trend Anal Chem* 166:117205
 17. Wang Y, Wei T-X (2013) Surface plasmon resonance sensor chips for the recognition of bovine serum albumin via electropolymerized molecularly imprinted polymers. *Chinese Chem Lett* 24:813–816
 18. Matyjaszewski K (2018) Advanced materials by atom transfer radical polymerization. *Adv Mater* 30:1706441
 19. Li Q, Zhang W, Liu X, Zhang H (2022) Preparation of complex biological sample-compatible “turn-on”-type ratiometric fluorescent molecularly imprinted polymer microspheres via one-pot surface-initiated ATRP. *Microchim Acta* 189:464
 20. Li X, Pan J, Dai J, Dai X, Xu L, Wei X, Hang H, Li C, Liu Y (2012) Surface molecular imprinting onto magnetic yeast composites via atom transfer radical polymerization for selective recognition of cefalexin. *Chem Eng J* 198–199:503–511
 21. Peng Z, Han X, Li S, Al-Youbi AO, Bashammakh AS, El-Shahawi MS, Leblanc RM (2017) Carbon dots: biomacromolecule interaction, bioimaging and nanomedicine. *Coordin Chem Rev* 343:256–277
 22. Zhu X, Yuan X, Han L, Liu H, Sun B (2021) A smartphone-integrated optosensing platform based on red-emission carbon dots for real-time detection of pyrethroids. *Biosens Bioelectron* 191:113460
 23. Wang R, Lu K-Q, Tang Z-R, Xu Y-J (2017) Recent progress in carbon quantum dots: synthesis, properties and applications in photocatalysis. *J Mater Chem A* 5:3717–3734
 24. Roy P, Chen P-C, Periasamy AP, Chen Y-N, Chang H-T (2015) Photoluminescent carbon nanodots: synthesis, physicochemical properties and analytical applications. *Mater Today* 18:447–458
 25. Wu Q, Wang X, Rasaki SA, Thomas T, Wang C, Zhang C, Yang M (2018) Yellow-emitting carbon-dots-impregnated carboxy methyl cellulose/poly-vinyl-alcohol and chitosan: stable, free-standing, enhanced-quenching Cu^{2+} -ions sensor. *J Mater Chem C* 6:4508–4515
 26. Hao J, Wang F, Dai X, Gong B, Wei Y (2011) Preparation of poly(vinyltetrazole) chain-grafted poly(glycidymethacrylate-co-ethylenedimethacrylate) beads by surface-initiated atom transfer radical polymerization for the use in weak cation exchange and hydrophilic interaction chromatography. *Talanta* 85:482–487
 27. Bai Q, Huang C, Ma S, Gong B, Ou J (2023) Rapid adsorption and detection of copper ions in water by dual-functional ion-imprinted polymers doping with carbon dots. *Sep Purif Technol* 315:123666
 28. Wang H, Huang C, Ma S, Guo S, Gong B, Ou J (2023) Fabrication of bifunctional macroporous adsorption resin via grafting carbon dot and application in the detection and adsorption of iron (III) ion. *Mater Today Commun* 34:105220
 29. Cai T, Zhou Y, Liu H, Li J, Wang X, Zhao S, Gong B (2021) Preparation of monodisperse, restricted-access, media-molecularly imprinted polymers using bi-functional monomers for solid-phase extraction of sarafloxacin from complex samples. *J Chromatogr A* 1642:462009
 30. Jalili R, Khataee A, Rashidi MR, Razmjou A (2020) Detection of penicillin G residues in milk based on dual-emission carbon dots and molecularly imprinted polymers. *Food Chem* 314:126172
 31. Pupin RR, Foguel MV, Gonçalves LM, Sotomayor M, d P T, (2019) Magnetic molecularly imprinted polymers obtained by photopolymerization for selective recognition of penicillin G. *J Appl Polym Sci* 137:48496
 32. Rahim ZA, Yusof NA, Ismail S, Mohammad F, Abdullah J, Rahman NA, Abubakar L, Soleiman AA (2023) Functional nano molecularly imprinted polymer for the detection of penicillin G in pharmaceutical samples. *J Polym Res* 30:113
 33. Rahdar S, Rahdar A, Khodadadi M, Ahmadi S (2019) Error analysis of adsorption isotherm models for penicillin G onto magnesium oxide nanoparticles. *Appl Water Sci* 9:190
 34. Lu X, Xing H, Su B, Yang Y, Ren Q (2009) Adsorption behavior of penicillin G sodium on hydrophilic gel toyopearl HW-40F. *J Chem Eng Data* 54:1052–1053
 35. Li X, Zhang N, Yang L (2020) Adsorption of ampicillin sodium on activated carbons with different surface chemistries. *IOP Conf Ser: Earth Environ Sci* 467:012184

Publisher's Note Springer Nature remains neutral with regard to jurisdictional claims in published maps and institutional affiliations.

Springer Nature or its licensor (e.g. a society or other partner) holds exclusive rights to this article under a publishing agreement with the author(s) or other rightsholder(s); author self-archiving of the accepted manuscript version of this article is solely governed by the terms of such publishing agreement and applicable law.